J Mol Model (2011) 17:1259–1265
DOI 10.1007/s00894-010-0822-5

ORIGINAL PAPER

Identification of ligand binding site on RXRγ using molecular docking and dynamics methods

Peng Zhao · Qing-hua Liao · Cheng-Feng Ren · Jing Wei

Received: 22 April 2010 / Accepted: 26 July 2010 / Published online: 26 August 2010

Abstract Retinoid X receptors (RXRα, β and γ) are recently known to be cancer chemotherapies targets. The ligand binding domains of RXRs have been crystallized, but the information of RXRγ ligand binding site is not yet available due to the lack of liganded complex. A thorough understanding of the ligand binding sites is essential to study RXRs and may result in cancer therapeutic breakthrough. Thus we aimed to study the RXRγ ligand binding site and find out the differences between the three subtypes. Alignment and molecular simulation were carried out for identifying the RXRγ ligand binding site, characterizing the RXRγ ligand binding mode and comparing the three RXRs. The result has indicated that the RXRγ ligand binding site is defined by helices H5, H10, β-sheet s1 and the end loop. Besides hydrophobic interactions, the ligand 9-cis retinoic acid interacts with RXRγ through a hydrogen bond with Ala106, a salt bridge with Arg95 and the π-π interactions with Phe217 and Phe218. The binding modes exhibit some similarities among RXRs, such as the interactions with Arg95 and Ala106. Nonetheless, owing to the absence of Ile47, Cys48, Ala50, Ala51 and residues 225~237 in the active site, the binding pocket in RXRγ is two times larger than those of RXRα and RXRβ. Meanwhile, spatial effects of Trp84, Arg95, Ala106, Phe217 and Phe218 help to create a differently shaped binding pocket as compared to those of RXRα and RXRβ. Consequently, the ligand in RXRγ undergoes a "standing" posing which is distinct from the other two RXRs.

P. Zhao · Q.-h. Liao · C.-F. Ren · J. Wei (✉)
Tianjin Key Laboratory for Modern Drug Delivery & High-Efficiency, School of Pharmaceutical Science and Technology, Tianjin University,
92 Weijin Road, Nankai District,
Tianjin 300072, People's Republic of China
e-mail: betty_wj@tju.edu.cn

Keywords 9-cis retinoic acid · Ligand binding site · Molecular docking · Molecular dynamics simulation · Retinoid X receptor

Introduction

The retinoid X receptor (RXR) is one member of nonsteroidal nuclear hormone receptor superfamily that is activated by vitamin A metabolite 9-cis retinoic acid (9cRA) [1, 2]. Three subtypes of RXRs have been identified: α, β and γ, each with different gene-code and specific tissue distribution [3]. Working as monomers or dimmers by themselves or heterodimers with other nuclear receptors such as retinoic acid receptor (RAR), the RXRs are playing important roles in a variety of physiological events including embryo development, organogenesis, and regeneration [4]. They are now under investigation as targets for cancer chemotherapies [3, 5].

Understanding the information about RXR ligand binding sites and the respective ligand binding modes of the three subtypes is an essential step in the development of new anti-tumor drug. To date, the X-ray crystal structures of the RXR ligand binding domains (LBDs) have been independently determined [6–8]. The RXRα and RXRβ LBDs are solved in complex with the ligands while the RXRγ LBD is released without a ligand. These crystal structures reveal that the RXRα and RXRβ share a similar ligand binding site. However, the difference of ligand binding properties between RXRs remains an open question in the absence of a ligand-bound RXRγ complex.

Computer-aided simulation of protein-ligand interactions can often be of great help in guiding and interpreting experiments, and can provide atomic details that are inaccessible using other experimental techniques [9]. In

our study, the techniques of alignment and molecular simulation (molecular docking and molecular dynamics (MD) simulation) were used to locate the RXRγ ligand binding site and predict its ligand binding mode. Meanwhile, the comparison of the three RXRs in ligand binding modes was preformed. It is hoped the information from this study will provide further understanding of RXRγ and illuminate the differences in ligand binding modes among the three RXR subtypes.

Materials and methods

Molecular structures

Human retinoic acid receptor RXRγ LBD (PDB code: 2GL8) with resolution 2.40 Å was obtained from Protein Data Bank [10]. The crystal structure is a symmetric tetramer that has ten helices and two β-sheets s1, s2 per each of its four monomers (A, B, C and D monomers) [6]. Monomer A was used as the docking receptor. Several side chains of amino acids were missing, and the reconstruction process was preformed using facilities within the Swiss-PdbViewer package [11]. The natural ligand 9cRA was taken as the docking ligand, and its structure was extracted from the crystal structure of the *holo*-RXRα LBD (PDB code: 1FBY).

Automated docking

Docking simulation to bind the 9cRA into RXRγ LBD was carried out using the AutoDock 4.0 program [12]. The AutoDock program could select the correct protein-ligand complexes based on the binding free-energy [13, 14]. Docking simulation was done using the Lamarckian genetic algorithm (LGA) [12]. A population size of 150 and 2,500,000 energy evaluations were used for 100 search runs. The docking area was defined by a box, with grid spacing of 0.375 Å and the dimension of 120×110×110 points along the x, y and z axes. The docking results from each of the 100 calculations were ranked according to the binding free energy. The conformation with the lowest docked energy was chosen and put through the MD simulation.

Molecular dynamics simulation

Amber 10.0 software [15] was used for MD simulation. Based on the docking result, MD simulation of the RXRγ LBD/9cRA system was performed using the SANDER module, implemented in the Amber 10.0 package. The Amber parm99SB force field [16] and the general AMBER force field (GAFF) [17] were respectively used for the protein and the ligand. The force field parameters of 9cRA were prepared with the Antechamber module [18]. The complex was solved in the TIP3P water box [19], with each side 7 Å from the edge of the complex. Counter ions (Na+) were added to neutralize the charge of system. The particle mesh Ewald (PME) method [20] was used to treat long-range electrostatic interactions. The SHAKE algorithm [21] was applied to fix all covalent bonds containing a hydrogen atom. The solvated system was energy-minimized prior to the MD simulation. First of all, the protein-ligand was frozen and the solvent water molecules with the counterions were allowed to move. Next, the ligand and the receptor residues were allowed to move in addition to the water molecules. Finally, all atoms were permitted to move freely. In each step, energy minimization was executed by the steepest descent method for the first 5,000 steps and the conjugated gradient method for the subsequent 2,500 steps. Subsequently, the complex of the minimized structures was subjected to a 12 ns MD simulation at 300 K and 1 atm pressure with an integration step of 2 fs and NPT as an ensemble type. The MD simulation was performed with a periodic boundary condition. Trajectories were analyzed using the PTRAJ modules [22]. To analyze the stability of the MD simulation, we plotted the RMSD values relative to the initial structure of the RXRγ backbone atoms during the 12 ns MD simulation against time.

Results and discussion

Ligand binding site of RXRγ

It is generally held that the three RXRs share a modular architecture that includes one ligand binding site. It contains the ligand-induced transcriptional activation function AF-2 [23]. Multiple amino acid sequence alignment of RXRα, RXRβ and RXRγ was preformed by ClustalX 1.83 program [24]. The alignment has shown that the residues defining the ligand binding site of the three RXRs are well conserved. Furthermore, a superimposition of RXRγ LBD structure with those of RXRα and RXRβ has indicated that the ligand binding site in RXRγ is located in the central core of the LBD, flanked by helices H5, H10, β-sheet s1 and the end loop (residues 214~224). Remarkably, the combined sequence alignment and structure superimposition have indicated that residues Ala50 and Ala51 reserved in RXRγ can not be classified as binding residues because they are out of the active binding area, while the corresponding residues in the other two subtypes locate in the binding area. Figure 1 shows the result of sequence alignment.

Ligand binding mode of RXRγ

The combination of docking and MD simulation is promising for characterizing the ligand binding mode in

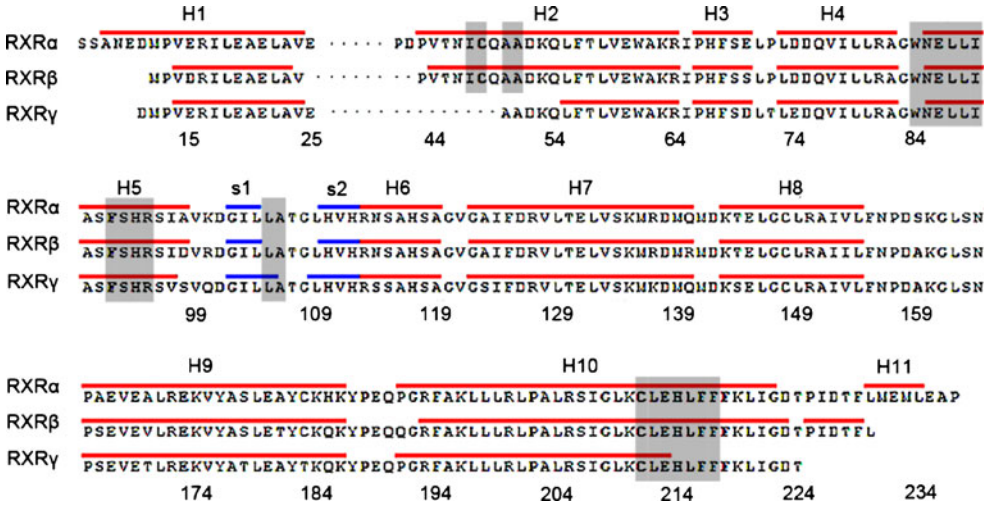

Fig. 1 Amino acids sequences alignment of RXRα, RXRβ and RXRγ LBDs. The three lines indicate the amino acids sequences of RXRα, RXRβ and RXRγ, respectively. The gaps are represented by (·) where there are absences of amino acid residues. The amino acids that compose α-helices are marked under red bars and β-sheets under blue bars. The ligand binding residues conserved among the RXRs are enclosed in gray boxes

protein. When predicting the posing of a ligand into a protein, docking can provide a good starting point for further calculations with the aim of evaluating the stability of the predicted interactions involved in binding. Further calculation is undertaken performing MD simulation to consider the effects of the receptor flexibility and the explicit water solvation on the complex of interest.

Docking simulation was firstly carried out to bind 9cRA into the RXRγ LBD structure. The most favorable conformation (the one with the lowest docked energy) found in the 100 independent docking runs was used as the starting structure of 9cRA in the MD simulation. After a 12 ns MD simulation for the complex, the system became equilibrated judged by the total energies' changing trends. In order to evaluate the stability of the complex, several parameters were monitored during the simulations. These include (1) RMSDs from starting structure for the Cα, C and N atoms of the receptor, the ligand as well as their complex, (2) the interactions between the ligand and the receptor.

The RMSD fluctuations of backbone atoms compared with the initial structure were obtained. Figure 2 shows the RMSD of the receptor, the ligand and their complex as a function of time. It can be seen that the receptor, the ligand and the complex have a relatively smooth curve in the last 2 ns with the mean RMSD values of 3.53 Å, 2.05 Å and 3.16 Å, respectively. This was confirmed by the examination of the interval conformations using VMD software [25], which displayed that the ligand was always anchored into the active site during the whole dynamic processes. After 12 ns simulation, the system reach equilibrium and the trajectories can be applied to collect snapshots for further analyses.

The final snapshot obtained by the MD simulations was used to study the interactions between 9cRA and RXRγ. Consequently, it is found that there are hydrophobic interactions, π-π interactions, a hydrogen bond and a salt bridge between 9cRA and RXRγ. These interactions are represented in Fig. 3.

The 9cRA makes extensive contacts with RXRγ LBD. The majority of contacts are hydrophobic interactions. The unsaturated β-ionone ring makes hydrophobic contacts with residues Trp84, Leu88, Ile89, Cys211 and Leu212. Residues Leu88 and Ile89 play a key role by interacting with the methyl groups at positions 16 and 17. The central hydrophobic part of the 9cRA is in close contact with Phe92, Leu105, Leu215, Phe217 and Phe218. The residues of Phe217 and Phe218 form favorable π-π interactions with the central conjugated part. This possibly plays an essential role in stabilizing protein-ligand complexes. In addition, the carboxyl group of the 9cRA accepts one hydrogen bond from the backbone amide of Ala106. We investigated the geometry and stability of this hydrogen bond on the basis of the trajectories of the MD simulation. The residue

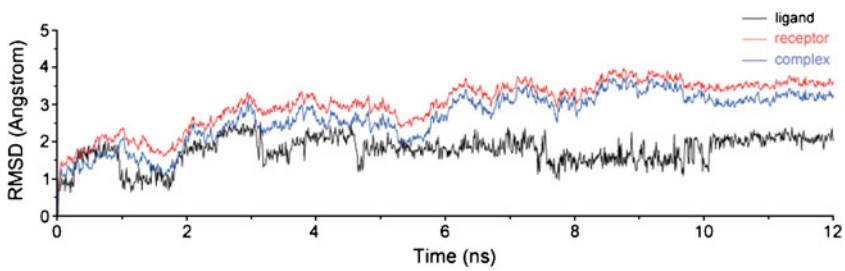

Fig. 2 The RMSDs from the starting structures calculated along the trajectory for the ligand 9cRA (black line), the receptor RXRγ LBD (red line) and the complex (blue line)

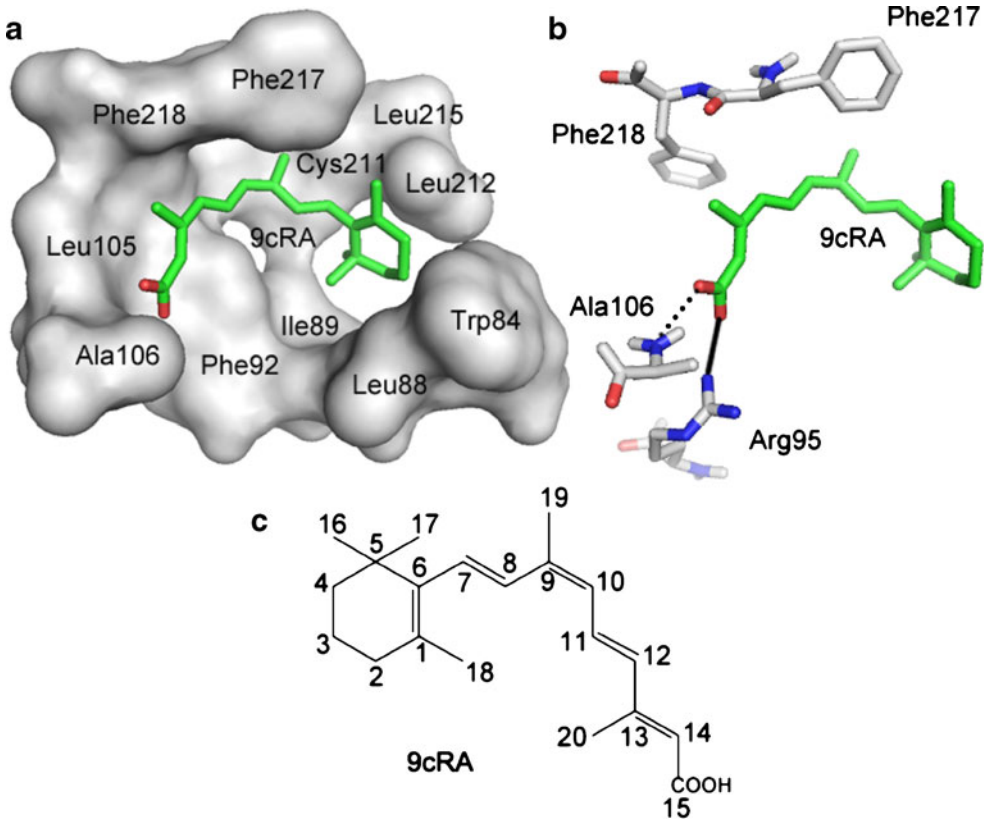

Fig. 3 The ligand binding modes of 9cRA in RXRγ. For clarity reasons only interacting residues are displayed. 9cRA (green) is represented as stick model. (**a**) Hydrophobic surface (pale gray) constructed by hydrophobic residues that interact with the ligand. (**b**) Representation of the hydrogen bond, the salt bridge and the π-π interaction. (**c**) The chemical structure of 9cRA. The hydrogen bond is shown by dotted black lines. Salt bridge is shown as black line. The interacting residues (white) Arg95, Ala106, Phe217 and Phe218 are represented as stick models

Ala106 makes one hydrogen bond (characterized in terms of distances between heavy atoms) through its nitrogen to the 9cRA carboxyl oxygen atom with average bond length of 2.948 Å (99% occupied of the bonds being maintained during the MD simulation). The profitable hydrogen bond could play an important role in defining the interaction pathway between 9cRA and residue Ala106. The nitrogen atom of Arg95 forms a salt bridge (2.886 Å in length) with hydroxyl oxygen atoms in the carboxyl end of 9cRA. Its function is not only the stability of ligand but also the fine tuning of ligand orientation in the active sites. Therefore, this complex is stable since Arg95 and Ala106 are holding the tail of the 9cRA while Trp84, Leu88, Ile89, Cys211 and Leu212 are anchoring the head.

Comparison of the ligand binding modes of RXRα, RXRβ and RXRγ

The information of protein-ligand binding sites is very important not only for revealing true binding mechanisms but also for rational drug design [26–29]. Molecular insight into the differences of RXRs and respective ligand binding properties may facilitate the design of RXR subtype-selective anti-tumor drug. Our comparative study involved the structures of three RXRs. The structure of 9cRA liganded RXRα LBD (PDB ID: 1FBY) was gained from the Protein Data Bank. The final snapshot generated in the MD simulation of RXRγ LBD was used as the structure of 9cRA bounded RXRγ LBD. The X-ray structure of RXRβ LBD (PDB ID: 1H9U) has been presented with a selective agonist LG268, but not the natural ligand 9cRA. We carried out a docking simulation with 9cRA and the RXRβ *apo*-LBD using AutoDock 4.0 software and consequently obtained the structure of RXRβ LBD in complex with 9cRA, thus allowing the comparison of the binding properties of the three RXRs.

The superimposition of the ligand binding sites indicates that the three subtypes have some similarities in ligand binding modes. The similarity extends to the presence of hydrogen bonds between 9cRA and the three RXRs. The carboxyl group of 9cRA participates in one hydrogen bond (2.948 Å in length) involving residue Ala106 in RXRγ. Similar hydrogen bonds (2.616 Å and 2.757 Å in length) can be discovered in RXRα:9cRA and RXRβ:9cRA complexes, respectively. Meanwhile, a salt bridge between the nitrogen atom of Arg95 and the carboxyl oxygen atom of 9cRA is conserved among the three RXRs. The one in RXRγ:9cRA complex is 2.886 Å long. The length of the corresponding salt bridge in RXRα:9cRA complex is 2.616 Å and that in RXRβ:9cRA complex is 2.757 Å. Calculated RMSD values for the ligand binding residues of RXRs from the structure alignment are given in Table 1.

RXRβ ligand binding site exhibits minor difference from that of RXRα with a RMSD (for the heavy atoms) of

only 0.450 Å. The percent of similarity between RXRα and RXRβ sequences, calculated by BioEdit program [30], is 87.1%. All of the pocket residues undergo tiny conformation rearrangements. As can be seen in Fig. 4a, the mercapto group of residue Cys211 in RXRβ swings 102.6°by comparison with that of RXRα. Due to the steric hindrance of this mercapto group, the β-ionone ring of 9cRA spins counterclockwise 43.9°about the C6-C7 bond compared with the pose in RXRα.

Nonetheless, RXRγ shows an obvious difference in sequence identity along with residues positioning when compared with the other two subtypes. The RMSD between RXRα and RXRγ ligand binding sites is 4.69 Å, and that between RXRβ and RXRγ is 4.47 Å. The sequence similarity between RXRα and RXRγ is 80.2%, and the similarity between RXRβ and RXRγ is 84.2%.

The analysis of sequences and structures suggests that the absence of residues Ile47, Cys48, Ala50 and Ala51 in RXRγ ligand binding site is one reason for the difference in ligand binding mode observed between the three RXRs. It can been found in Fig. 1 that RXRγ lacks residues Ile47 and Cys48 which help restrict the binding pocket in the other two subtypes. Meanwhile, Ala50 and Ala51 of RXRγ are positioned remote from the binding site and make no contact to the main body of 9cRA. Figure 4a has displayed residues Ile47, Cys48, Ala50 and Ala51 (in magenta) in RXRα and RXRβ as a comparison to RXRγ in Fig. 4b. Besides, the lack of residues 225~237 has contributed to create an unsealed cavity in RXRγ LBD. Together these differences result in a larger ligand binding cavity in RXRγ binding site to allow the free movement of 9cRA. The accessible volume of this cavity is 1986.1 $Å^3$. The corresponding residues in RXRα and RXRβ create enclosed and more globular cavities with the volume of 991.4 $Å^3$ and 743.2 $Å^3$, respectively. The probe-occupied ligand cavities were calculated by the tool of CASTp [31] with a probe radius of 1.4 Å.

The superimposition of the key binding residues of the three complexes (Fig. 4b) reveals that these residues in RXRγ adopt significantly different conformations compared with those in RXRα and RXRβ. These residues have high RMSD values as shown in Table 1. In particular, Phe217 and Phe218 adopt significantly different conformations in RXRγ with RMSD values over 9 Å. A shift of these two residues toward the center of the cavity is observed in RXRγ ligand binding site when compared with the other two subtypes. As a result, the 9cRA adopts a different relative orientation with a rotation of 158°around an axis roughly vertical to helix H2. The carboxyl group moves left and the β-ionone ring points upward, whereas in the other two subtypes, the β-ionone ring points to the bottom of the pocket. Meanwhile, residues Arg95 and Ala106 adjust their positions toward the left so as to interact with the carboxyl group of 9cRA. These rearrangements help to anchor the tail of the ligand, thus allowing the existence of this "standing" ligand conformation. Furthermore, Trp84 in RXRγ ligand binding site steers right with a RMSD over 2 Å, increasing the volume of the cavity. The flexibility of the Tryptophan residue allows such movement. It has reduced the steric hindrance to the β-ionone ring of 9cRA and further enhances the stability of this ligand conformation. Consequently, the ligand adopts the conformation shown in Fig. 4b.

Conclusions

The goal of this study was to elucidate the ligand binding site of RXRγ and rationally illuminate the ligand binding

Table 1 Calculated RMSD values[a] for the ligand binding residues of RXRs

Residues	Calculated in Pairs		
	RXRα : RXRβ	RXRα : RXRγ	RXRβ : RXRγ
Whole binding residues[b]	0.450	4.690	4.470
Ile47[c]	0.415	-	-
Cys48[c]	0.311	-	-
Ala50s[c]	0.368	-	-
Ala51[c]	0.193	-	-
Trp84	0.217	2.450	2.285
Leu88	0.149	0.856	0.741
Ile89	0.217	0.962	0.760
Arg95	0.595	3.940	3.791
Ala106	0.741	3.823	3.535
Cys211	0.440	0.835	0.881
Leu212	0.318	1.865	1.953
Phe217	0.802	9.936	9.331
Phe218	1.209	9.983	9.046

[a] All values are calculated by program SwissPdb Viewer and are given in Å

[b] RMSD values of the whole binding residues in the pocket

[c] Due to the absence of residues Ile47, Cys48, Ala50 and Ala51in RXRγ ligand binding site, the RMSD values of these residues between RXRγ and RXRα/β can not be calculated

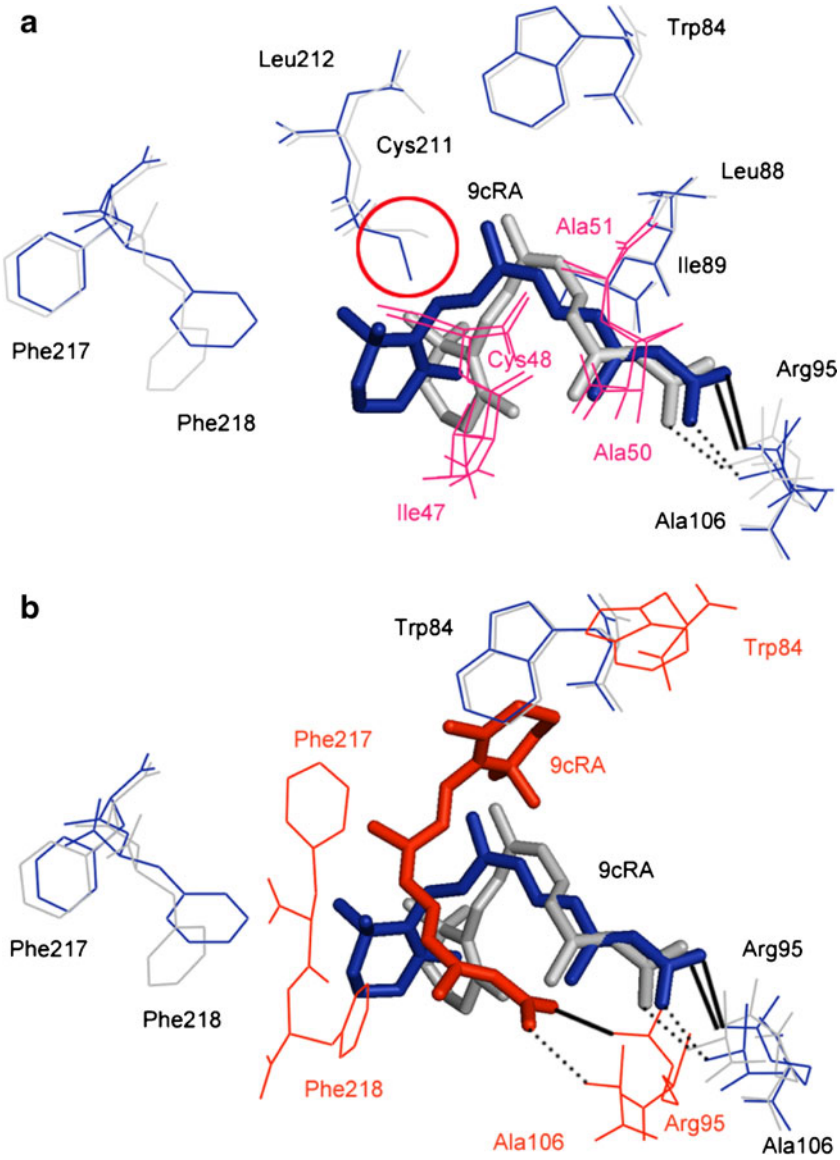

Fig. 4 A stereo view of the superimpositions of RXRα, RXRβ and RXRγ ligand binding residues. (**a**) Superposition of RXRα (blue) key binding residues against that of RXRβ (pale gray). Residues Ile47, Cys48, Ala50 and Ala51 are locating ahead of the 9cRA. To emphasize their positions, these residues are displayed and shown in magenta. (**b**) Key binding residues of RXRγ (red) superimposed with those of RXRα (blue) and RXRβ (pale gray). The ligands and residues are presented in stick and line models, respectively. Hydrogen bonds are shown by black dotted lines and the salt bridges are shown by black lines. For the sake of clarity, the residues have minor influence on the ligand binding are not displayed

differences of the three RXRs. Our study has indicated that the ligand binding site in RXRγ is a hydrophobic cavity formed by helices H5, H10, β-sheet s1 and the end loop. Besides the hydrophobic interactions, 9cRA interacts with RXRγ through a hydrogen bond, a salt bridge and the π-π interactions. The ligand binding modes exhibit some conserved features between the RXRγ and the other two subtypes, such as the interactions with Arg95 and Ala106 which could play a role in stabilizing the carboxyl group in the 9cRA. Nonetheless, the 9cRA adopts a "standing" orientation in RXRγ with the carboxyl group moves toward the left and the β-ionone ring points upward compared with the other two subtypes. This is a result of the differences in ligand binding sites between RXRγ and the other two RXRs. The binding pocket of RXRγ is two times larger than those of RXRα and RXRβ. The absence of residues Ile47, Cys48, Ala50, Ala51 and residues 225~237 in the active site of RXRγ help to enlarge the binding pocket. Besides, RXRγ employs a differently shaped ligand binding pocket due to the spatial effect of the binding residues. Arg95 and Ala106 move toward the left, while Trp84, Phe217 and Phe218 steer right. These have combined to create a pocket that accommodates the "standing" conformation of the ligand 9cRA.

The calculation reveals the difference between the RXRγ and the other two subtypes in volume and shape of the ligand binding site, offering interesting possibilities for the design of new, more specific RXR subtype-selective ligand. The size of such ligand is critical, for example, adding some suitable bulky groups at the ligand may develop a specific ligand for RXRγ.

Acknowledgments We gratefully acknowledge the support from Project of Undergraduate Educational Reform & Capacities in Tianjin University (No. 200904050).

References

1. Budhu AS, Noy N (2000) On the role of the carboxyl-terminal helix of RXR in the interactions of the receptor with ligand. Biochemistry 39:4090–4095. doi:10.1021/bi992827f
2. Lee WY, Noy N (2002) Interactions of RXR with coactivators are differentially mediated by helix 11 of the receptor's ligand binding domain. Biochemistry 41:2500–2508. doi:10.1021/bi011764+
3. Takamatsu K, Takano A, Yakushiji N, Morishita K, Matsuura N, Makishima M, Tai A, Sasaki K, Kakuta H (2008) The first potent subtype-selective retinoid X receptor (RXR) agonist possessing a 3-isopropoxy-4- isopropylphenylamino moiety, NEt-3IP (RXRα/β-dual agonist). Chem Med Chem 3:780–787. doi:10.1002/cmdc.200700313
4. Hopkins PM, Durica D, Washington T (2008) RXR isoforms and endogenous retinoids in the fiddler crab, Uca pugilator. Comp Biochem Physiol A Mol Integr Physiol 151:602–614. doi:10.1016/j.cbpa.2008.07.021
5. Tallafuss A, Hale LA, Yan YL, Dudley L, Eisen JS, Postlethwait JH (2006) Characterization of retinoid-X receptor genes rxra, rxrba, rxrbb and rxrg during zebrafish development. Gene Expr Patterns 6:556–565. doi:10.1016/j.modgep.2005.10.005
6. Schuetz A, Min JR, Loppnau P, Weigelt J, Sundstrom M, Edwards AM, Arrowsmith CH, Bochkarev A, Plotnikov AN (2006) The crystal structure of human retinoic acid receptor RXR-gamma ligand-binding domain. Toronto, Canada. doi:10.2210/pdb2gl8/pdb
7. Egea PF, Mitschler A, Rochel N, Ruff M, Chambon P, Moras D (2000) Crystal structure of the human RXRα ligand binding domain bound to its natural ligand: 9cRA. The EMBO Journal 19:2592–2601. doi:10.1093/emboj/19.11.2592
8. Love JD, Gooch JT, Benko S, Li C, Nagy L, Chatterjee VK, Evans RM, Schwabe JW (2002) The structural basis for the specificity of retinoid-X receptor-selective agonists: New insights into the role of Helix 12. J Biol Chem 277:11385–11391. doi:10.1074/jbc.M110869200
9. Miao J, Chapman HN, Kirz J, Sayre D, Hodgson KO (2004) Taking X-ray diffraction to the limit: macromolecular structures from femtosecond X-ray pulses and diffraction microscopy of cells with synchrotron radiation. Annu Rev Biophys Biomol Struct 33:157–176. doi:10.1146/annurev.biophys.33.110502.140405
10. Berman HM, Westbrook J, Feng Z, Gilliland G, Bhat TN, Weissig H, Shindyalov IN, Bourne PE (2000) The Protein Data Bank. Nucleic Acids Res 28:235–242. doi:10.1093/nar/28.1.235
11. Guex N, Peitsch MC (1997) Swiss-model and the Swiss-PdbViewer: an environment for comparative protein modeling. Electrophoresis 18:2714–2723. doi:10.1002/elps.1150181505
12. Morris GM, Goodsell DS, Halliday RS, Huey R, Hart WE, Belew RK, Olson AJ (1998) Automated docking using a Lamarckian genetic algorithm and an empirical binding free energy function. J Comput Chem 19:1639–1662. doi:10.1002/(SICI)1096-987X(19981115)19:14<1639::AID-JCC10>3.0.CO;2-B
13. Hetényi C, van der Spoel D (2002) Efficient docking of peptides to proteins without prior knowledge of the binding site. Protein Sci 11:1729–1737. doi:10.1110/ps.0202302
14. Huey R, Morris GM, Olson AJ, Goodsell DS (2006) A semiempirical free energy force field with charge-based desolvation. J Comput Chem 28:1145–1152. doi:10.1002/jcc.20634
15. Case DA, Cheatham TE 3rd, Darden T, Gohlke H, Luo R, Merz KM Jr, Onufriev A, Simmerling C, Wang B, Woods RJ (2005) The amber biomolecular simulation programs. J Comput Chem 26:1668–1688. doi:10.1002/jcc.20290
16. Hornak V, Abel R, Okur A, Strockbine B, Roitberg A, Simmerling C (2006) Comparison of multiple amber force fields and development of improved protein backbone parameters. Proteins 65:712–725. doi:10.1002/prot.21123
17. Wang JM, Wolf RM, Caldwell JW, Kollman PA, Case DA (2004) Development and testing of a general AMBER force field. J Comput Chem 25:1157–1174. doi:10.1002/jcc.20035
18. Wang J, Wang W, Kollman PA, Case DA (2001) Antechamber: an accessory software package for molecular mechanical calculations. Abstr Pap Am Chem Soc 222:U403
19. Jorgensen WL, Chandrasekhar J, Madura JD, Impey RW, Klein ML (1983) Comparison of simple potential functions for simulating liquid water. J Chem Phys 79:926–935. doi:10.1063/1.445869
20. Darden T, York D, Pedersen L (1993) Particle mesh ewald: an N-log(N) method for ewald sums in large systems. J Chem Phys 98:10089–10092. doi:10.1063/1.464397
21. Ryckaert JP, Ciccotti G, Berendsen HJC (1977) Numerical integration of the cartesian equations of motion of a system with constraints: molecular dynamics of n-alkanes. J Comput Phys 23:327–341. doi:10.1016/0021-9991(77)90098-5
22. Honig B, Nicholls A (1995) Classical electrostatics in biology and chemistry. Science 268:1144–1149. doi:10.1126/science.7761829
23. Chambon P (1994) The retinoid signaling pathway: molecular and genetic analysis. Semin Cell Biol 5:115–125. doi:10.1006/scel.1994.1015
24. Chenna R, Sugawara H, Koike T, Lopez R, Gibson TJ, Higgins DG, Thompson JD (2003) Multiple sequence alignment with the Clustal series programs. Nucleic Acids Res 31:3497–3500. doi:10.1093/nar/gkg500
25. Humphrey W, Dalke A, Schulten K (1996) VMD - Visual Molecular Dynamics. J Mol Graph 14:33–38. doi:10.1016/0263-7855(96)00018-5
26. Du QS, Huang RB, Wang CH, Li XM, Chou KC (2009) Energetic analysis of the two controversial drug binding sites of the M2 proton channel in influenza A virus. J Theor Biol 259:159–164. doi:10.1016/j.jtbi.2009.03.003
27. Chou KC, Jones D, Heinrikson RL (1997) Prediction of the tertiary structure and substrate binding site of caspase-8. FEBS Lett 419:49–54. doi:10.1016/S0014-5793(97)01246-5
28. Chou KC, Wei DQ, Zhong WZ (2003) Binding mechanism of coronavirus main proteinase with ligands and its implication to drug design against SARS. Biochem Biophys Res Commun 308:148–151. doi:10.1016/S0006-291X(03)01342-1
29. Wang SQ, Du QS, Huang RB, Zhang DW, Chou KC (2009) Insights from investigating the interaction of oseltamivir (Tamiflu) with neuraminidase of the 2009 H1N1 swine flu virus. Biochem Biophys Res Comm 386:432–436. doi:10.1016/j.bbrc.2009.06.016
30. Hall TA (1999) BioEdit: a user-friendly biological sequence alignment editor and analysis program for Windows 95/98/NT. Nucleic Acids Symp Ser 41:95–98
31. Dundas J, Ouyang Z, Tseng J, Binkowski A, Turpaz Y, Liang J (2006) CASTp: computed atlas of surface topography of proteins with structural and topographical mapping of functionally annotated resiudes. Nucleic Acids Res 34:W116–W118. doi:10.1093/nar/gkl282